Metallurgical and Materials Engineering *Research paper*
Association of Metallurgical Engineers of Serbia AMES *https://doi.org/10.30544/554*

EXPERIMENTAL STUDY OF FATIGUE DURABILITY IN BENDING EFFECT ON WELDED JOINTS IN STEEL PROFILES

Mohammad Ali Moslemi Petrudi [1,], Mehdi Saeed Kiasat [1], Manouchehr Fadavi [1], Amin Moslemi Petrudi [2]*

[1] Department of Maritime Engineering, Amirkabir University of Technology, Tehran, Iran
[2] Department of Mechanical Engineering, IHU University, Tehran, Iran

Received 27.08.2020
Accepted 22.02.2021

Abstract

Ships are always prone to fatigue through high periodic loads, usually caused by waves and changing load conditions. So, fatigue is an important factor in design. One of the reasons for fatigue in welding parts is variable bending loads. In this paper, a specimen of low-carbon steel T-Bar profiles is used, along with plates of the same type of steel that have been welded by the manual electrode welding process. To determine the distribution of static and dynamic forces created by welding, the specimens were subjected to bending (three-point loading) and tensile tests, and finally fatigue tests. The T-Bar Steel profile has more tolerance for fatigue loads than welded. The load T-Bar profile has not failed until the two million cycles, while the welding specimen has failed in about 3×10^5 cycles. Finally, strong penetrating welds should be used if a stronger welding joint is required.

Keywords: Three-Point Loading; High Cycle Fatigue (HCF); Tensile Test; Fatigue; T-Bar Profile.

Introduction

The fracture phenomenon is a destructive and accidental failures phenomenon in the design of structures. It is necessary that the relationship between external stress and the crack length in part is the material's properties and is very important in designing structures resistant to failure and control of this phenomenon. The history of engineering structures has witnessed numerous failures in machinery, automotive, welding structures, aircraft. These fatigue failures have led to a large number of accidents as well as significant economic losses. In the course of comprehensive research and practical experiments, a great deal of knowledge has been gained about fatigue in structures and the process of fatigue. One of the most important causes of disability and failure of parts

*Corresponding author: MohammadAli Moslemi Petrudi, *mamp_1394@yahoo.com*

is the phenomenon of fatigue. Fatigue is a local phenomenon that occurs as a result of the alternating application of alternating stresses. Failure analysis often reveals structural weaknesses that cause low fatigue resistance. One of the reasons for fatigue in welded sections is variable bending loads, which should be used to estimate the life of the weld under the variable load. Then, by applying wide and point loads in all cases and situations, it should be examined. The purpose of this paper is to study the stresses and fatigue fractures caused by bending forces applied to T Beam. Brittle fatigue occurs without any change in the impure shape of the fracture. The macroscopic fracture surface is usually perpendicular to the main tensile stress [1]. The fatigue fracture surface is distinguished from the appearance of the fracture surface, which consists of a smooth area resulting from abrasion with the onset of fragmentation and an uneven area that is a ductile failure in the workpiece when the load is not tolerated by the section [2, 3]. Failure of engineering components is usually of three types:

- Sudden brittle failure;
- Gradual and progressive fatigue or failure;
- Delayed failure.

Three major factors are essential for the failure of fatigue. These factors include:

- Maximum tensile stress;
- Stress range;
- The number of cycles.

Also, there are other variables such as stress concentration, corrosion, temperature, overload, metallurgical structure, residual stresses, and compound stresses that reinforce the conditions for fatigue. Carbon steels are a broad group of steels with a maximum carbon content of 1.7%, a manganese content of 65.6%, and a maximum of 0.6% silicon. There are no alloying elements such as chromium, nickel, molybdenum, etc., in these steels, or their amount is very small [4, 5, 6]. Specimen carbon steels can be divided into four groups:

- Low carbon steels with a maximum of 0.15% carbon;
- Steel with partial carbon (soft) with a maximum of 0.159% carbon;
- Carbon intermediate steels with 0.39% carbon;
- High-carbon steels with a maximum of 0.6% carbon.

In this study, low carbon steel has been used for welding the T-Bar profile specimen. Equivalent carbon is used to test the weldability of steel [7, 8]. The relationship first developed by *Dearden* and *O'Neill* adopted by the International Welding Institute in 1976 with some modifications is as follows:

$$CE = C + \frac{Mn}{6} + \frac{Cu + Ni}{15} + \frac{Cr + Mo + V}{5} \qquad 1$$

This relation is used for specimen carbon and manganese carbon steels but is not used in high-strength micro-alloy steels or micro-alloy steels [9, 10]. The acceptable relation between the Japanese welding engineering community, which was achieved by *Ito* and *Bessyo*, is relation 2.

$$P_{cm} = C + \frac{Si}{30} + \frac{Mn + Cu + Cr}{20} + \frac{Ni}{60} + \frac{Mo}{15} + \frac{V}{10} \qquad 2$$

In this relation, as in the carbon IIW equivalent, all elements are expressed in terms of mass percentage [11,12]. P_{cm} relies on a wider range of steels than IIW. P_{cm} is also called the chemical compound parameter [13]. According to AWS D 1.1, XI, the chemical composition parameter value can be used to predict the amount of hydrogen [14]. A study presented by the fatigue assessment of the welded joint was assessed using the finite element method. They suggested that it be used to examine the onset of cracks in cavities and the progress of cracks in the joint of discontinuous T-Bar profiles [15]. The starting point of the crack is a hole and a three-dimensional shape, and its development is simulated and enters the plastic elastic region of the weld metal until complete failure of the weld occurs [16]. Performed fatigue tests in three methods and the plate's direction with a welded joint are under bending load [17]. The results of fatigue tests performed on a one-way welded joint, a two-way weld joint, and a cross-shaped weld joint show that the fatigue crack shapes resemble flat ellipses that move along the weld line and up to about 80% of the thickness of the previous sheet it prevents failure [18]. The fatigue strength of the T-Bar profile welded joint under bending is greater than tensile strength. The aspect ratio, c/a, decreases during the crack progression stage and is then kept low until it reaches the failure stage because the small cracks merge at a time before the crack is long and the crack is slightly deeper. A comparison of the fatigue life progression of fatigue crack with the type of stress loading and bending is evaluated and shows that bending causes a longer distribution of fatigue life than stress. In two million load cycles, fatigue strength is 20% 12SS higher than 12SD and 12CR.In some, experiments and studies on small specimens did not have a clear answer. More in-depth studies on fatigue strength were performed by Frick et al. that included examining ship structures and built specimens in real dimensions. Two types of structures were selected for this study, one for the corner frame network for cargo ships and the other for a cross-sectional section for container ships, for which five specimens were tested. The specimens were connected by cross-linking. The five models tested included three models under constant load and two models under variable load. The experiment results showed that with fixed loading specimens, a longitudinal crack appeared in the upper beam. In the variable loading specimens, a long crack appeared during welding after the first crack. Also, conducted experiments to predict the fatigue life of welded joints with different values between the two test sheets. The results were obtained for the optimal distance between two sheets of 0 to 2 mm. Results showed that specimens with constant loading had a longitudinal crack in the upper joist. Specimens with variable loading a long crack appeared along with the welding after the first crack. Microstructure and mechanical properties of high-strength steel welding consumables with a minimum yield strength of 1100 MPa [19]. Numerical study of keyhole instability and porosity formation mechanism in laser welding of aluminum alloy and steel [20]. Comparative study of autogenous tungsten inert gas welding and tungsten arc welding with filler wire for dissimilar P91 and P92 steel weld joint [21]. Review of Aluminum-To-Steel Welding Technologies for Applications [22]. Metal Fatigue in Engineering [23]. *Moslemi Petrudi et al.* [24] numerical and analytical study of fatigue and degradation in multilayer composite plates. The present study and compares the results of this method with those of other researchers. Stress and damage contours have been reported. it is shown Change in the diameter of the central open-hole not only the effect on possible damage, damaging rate, progressive damage but also the effect on the strength of the composite laminates is also indicated. *Macek et al.* [25] effect of multiaxial bending-torsion loading on fracture surface parameters in high-strength

steels processed by conventional and additive manufacturing. In the first stage, combined bending-torsion fatigue tests are performed for three bending-to-torsion ratios. In a second stage, based on the entire total area method, fracture surfaces are analyzed via different surface topography parameters, namely height parameters, material/void volume parameters. The results show that surface topography parameters are decreasing functions of the bending-to-torsion ratio and fatigue life and increasing functions of von Mises stress range. *Macek et al.* [26] three-dimensional Fractography analysis of total fracture areas in 6082 aluminum alloy specimens under fatigue bending with controlled damage degree. This paper proposes a mixed mechanical-metrological approachable to account for the three-dimensional Fractography damage in samples subjected to fatigue bending loading histories based on the system dynamics. The results show a clear relationship between the changes in the recorded accelerations associated with the degree of fatigue damage and the texture parameters' values mentioned above. *Atak et al.* [28] investigate mechanical properties, and fatigue of friction stir spot welded light metals. Mechanical properties of joined materials such as tensile, tensile shear, bending, and fatigue strength were tested. As a result, it has been verified that light metal alloys such as magnesium alloy AZ31B with good ductile and fatigue strength can easily be joined with FSSW. Moreover, the joining of light metals with the FSSW method has been demonstrated with comparative tests and analyses in engineering applications. In this paper, a specimen of low-carbon steel T-Bar profiles is used, along with plates of the same type of steel that have been welded by the manual electrode welding process. Finally, strong penetrating welds should be used if a stronger welding joint is required.

Experimental Studies

In the present study, the structural steel St 37-2 plate (Standard DIN 17100) with the dimension of 250 mm × 50 mm and 5mm thickness sheet has been used. The chemical composition of the plate is given in Table 1.

Table 1. Chemical composition of the base metal by weight percentage (wt.%).

C	Si	Mn	P	S	Cu	Al
0.085	0.015	0.543	0.075	0.057	0.004	0.026
V	Ti	Nb	Co	Sn	Zr	Pb
0.001	0.001	0.001	0.001	0.005	0.001	0.001

According to relation 1, the carbon equivalent of this steel is equal to 0.204, so the desired steel has good welding capability. After preparing the mentioned sheets according to the dimensions and sizes are given in Figure 2, welding and build of the specimen were performed. Specimens with dimensions and material as the base metal, T-Bar profiled rolled profiles have also been used to compare the mechanical properties of the welded specimens. The sheet in the 450 × 300 mm dimensions, specimens in the size of 50 × 300 mm, and 40 × 300 mm were cut and prepared by the cutting machine. Also, for the preparation of T-Bar profile specimens, a T-Bar profile beam was mentioned in cross-sectional dimensions, and a length of 1500 mm was used. According to the prepared joint plan, the cut sheets are prepared by the chamfering machine for the welding stage. Figure 3 shows the design and the dimensions used for the top sheet. Then, to clean the desired parts for welding, the surface is completely cleaned by electric wire brushing. To create a welded joint with full penetration, the prepared sheets are assembled at a distance of 1

mm from each other and in 1F mode. The flat (1F) fillet position is performed where the fillet weld is rotated so that the filler material will be level with the ground. This is the easiest position and will only qualify you for the flat position. Figure 1 shows the welding position [29].

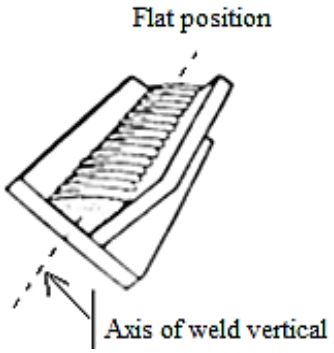

Fig 1. Welding position [29].

The electrodes were first welded together using the (AMA 2000) electrode AWS E 6013, and then the two ends of the specimen were welded with the same electrode to keep the workpiece fixed to the work table. Two electrodes AWS 8H- 7018 E (F 1230 AMA) electrodes with a diameter of 2.5 mm were used on each side to assemble the specimen. To prevent the specimen from swinging, after welding on one side, the specimen remained in the ambient air for 5 minutes. Figure 2 shows size and dimensions in the welded piece. Figure 3 shows joint of the joint for the sheet. Then the other side was welded by removing the joint to the work table and rotating the specimen. Figure 5 shows the specimen is joined to the workbench and welded. After welding and making a specimen 2.5 cm on both sides of the workpiece, it is cut and discarded by a fire cutter. The reason for this is to get a healthy weld from the workpiece. The cut of the welded specimen is shown in Figure 4 to perform the tensile test, and the required specimen was performed according to the standard ASTM –A370. The image of the final specimen is shown in Figure 6 to perform the static bending test on one of the welded specimens and one of the rolled specimens, equal to the given dimensions according to the standard AWS B4- 07 has been used. The vertical welded plate is cut on the workpiece to the welding surface and then machined to place the specimen and apply the load on the three-point bending machine. Figure 6 shows a design of the specimen prepared for the bending test.

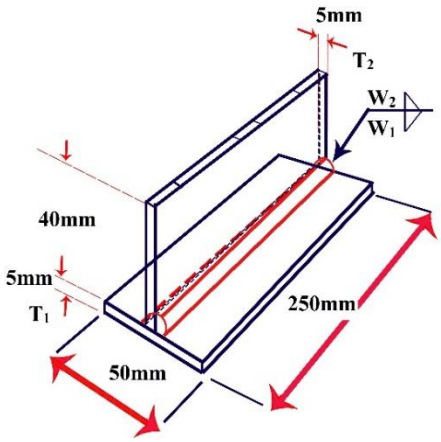

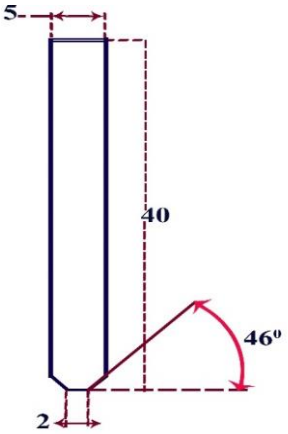

Fig 2. Size and dimensions in the welded piece. *Fig 3. Joint of the joint for the sheet.*

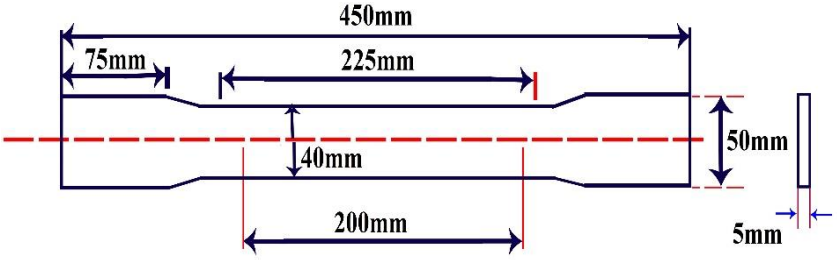

Fig 4. Specimen prepared for tensile tests.

Fig 5. Sheet assembly.

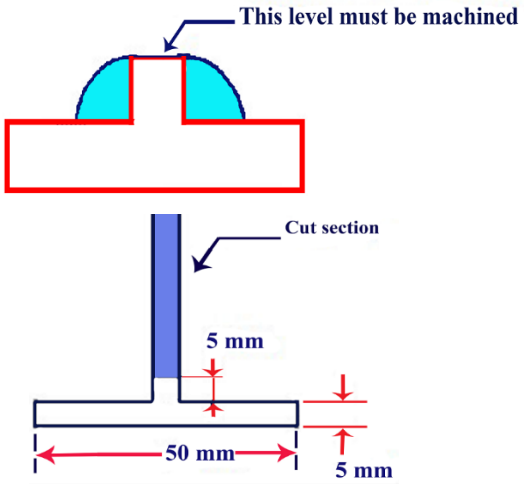

Fig 6. Designed specimen.

To perform the test, the specimen is first placed on the embedded fixture. This fixture consists of two cylinders with a diameter of 30 mm, which are secured using screws on the device's base. Another cylinder with a diameter of 31 mm is connected to the fixture. According to the bending test results, the selection value for the fatigue test and loading conditions is as described in Figure 7. The test continues until the workpiece fails or reaches 10^6 cycles. Figure 6 shows loading three points on a workpiece and the fatigue test.

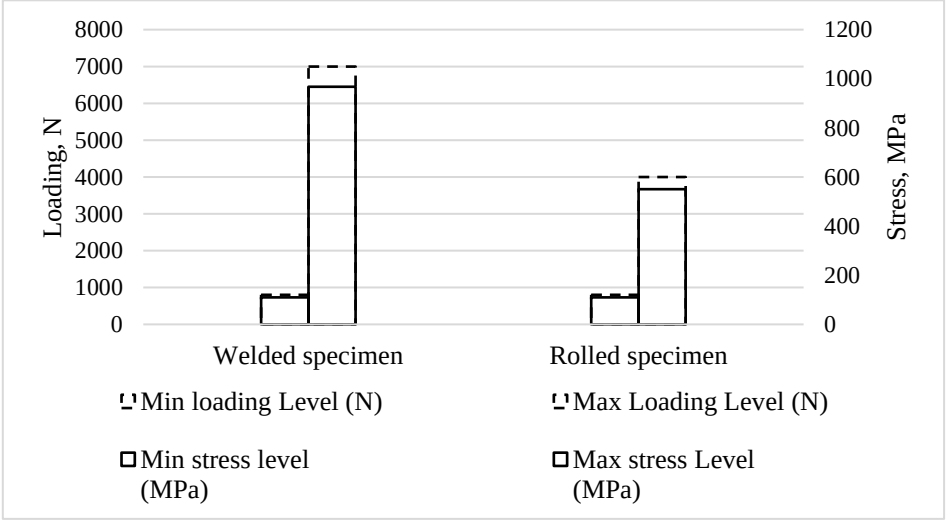

Fig. 7. Fatigue test conditions.

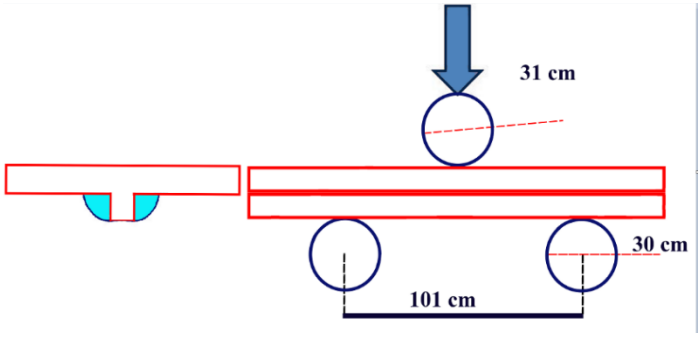

(a)

(b)

Fig 8. a) Loading type, b) Fatigue test machine, and the location of the specimen.

The Rockwell Hardness tests with a force of 100 kg and 1/16 inch-diameter steel ball were performed by the Rockwell HRR-150A hardness machine on the weld metal and rolled specimen. Also, to better evaluate the hardness, the hardness profile is drawn from the base metal to the top layer of the weld. The initial load of 10 kg of force was used to draw the hardness profile. To draw the hardness profile, it was performed at 6 points with a distance of 0.5 mm. Figure 8 The hardness of the base metal starts, and after it is done in the heat-affected area, the surface layer is finished in the weld metal. The origin of the movement is on the centerline. specimen's hardness test was performed at 23ºC and 35% humidity. The standard for testing was ASTM E 18-2015. Figure 9 shows the hardness profile on both welded and rolled specimens.

(b) (a)

Fig. 9. Hardness profile; a) welded specimen, b) rolled specimen.

A Shanghai Optics hardness machine was used to perform the hardness test. Then, the results of stiffness assessment were statistically investigated, and the following relations were used to express the mean value ($\bar{x}$), variance (S^2), standard deviation (S), and mean standard error ($S_{\bar{x}}$):

$$\bar{x} = \frac{\sum x}{n} \quad (3)$$

$$S^2 = \sqrt{\frac{\sum (x-\bar{x})^2}{n-1}} \quad (4)$$

$$S = \sqrt{S^2} = \sqrt{\frac{\sum (x-\bar{x})^2}{n-1}} \quad (5)$$

$$\bar{Y} = \frac{1}{A} \sum \bar{y}_i . A_i \quad (6)$$

$$S_{\bar{x}} = \frac{s}{\sqrt{n}} \quad (7)$$

In the above relations, x the amount of difficulty at each point (according to Rockwell) and n the number of points examined statistically are expressed. The loads

entered in the static bending and fatigue test are of Newtonian force. Using the following relations must first calculate the moment of inertia of each stressed surface and then measure the stress by using the relations of computation of the governing stress.

$$I_{x'} = \sum(\bar{I} + Ad^2) \quad (8)$$

$$\bar{I} = \frac{1}{12}bh^3 \quad \textit{(for Rectangular)} \quad (9)$$

$$\bar{I} = \frac{1}{36}bh^3 \quad \textit{(for Triangle)} \quad (10)$$

$$\sigma = \frac{MC}{I} \quad (11)$$

In the above relations $\bar{Y}$, is the center of the cross-sectional area of the specimen, $\bar{I}$ is the surface torque, and $I_{x'}$ is the total torque applied around the neutral axis, and σ is the amount of stress applied to the cross-sectional area.

Results

In the tensile test, after necking is observed, failure occurs in the specimen. The results of the strain-stress test for base metal tensile test for yield strength 324.4 MPa and ultimate tensile strength 458.5 MPa. The strain-stress diagram for the base metal is also shown in Figure 11. The diagrams obtained from this test for this test and also the combination of the two diagrams to compare the results are shown in Figure 12.

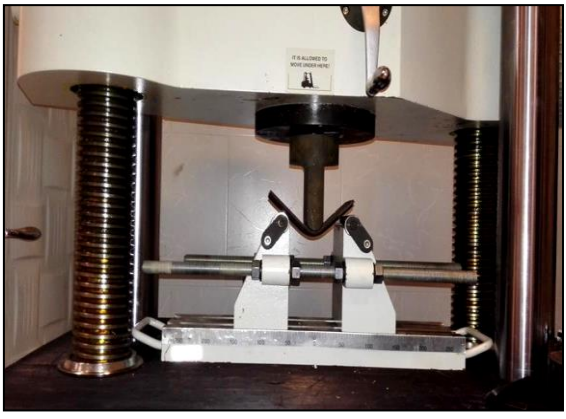

Fig. 10. Loading on the specimens in the static bending test.

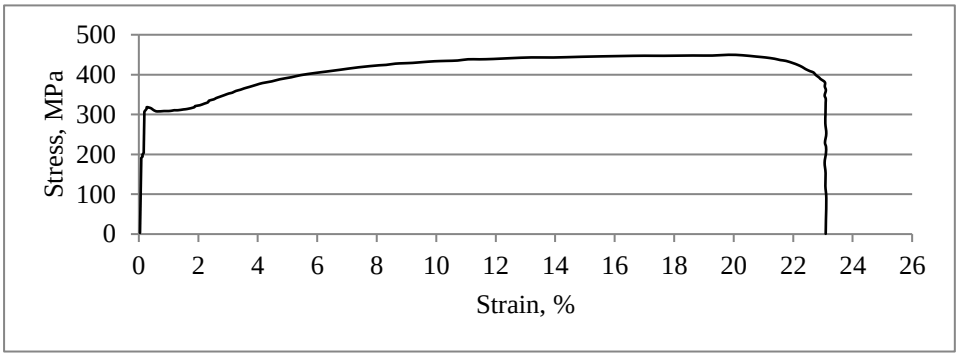

Fig. 11. Stress-strain diagram for the base metal.

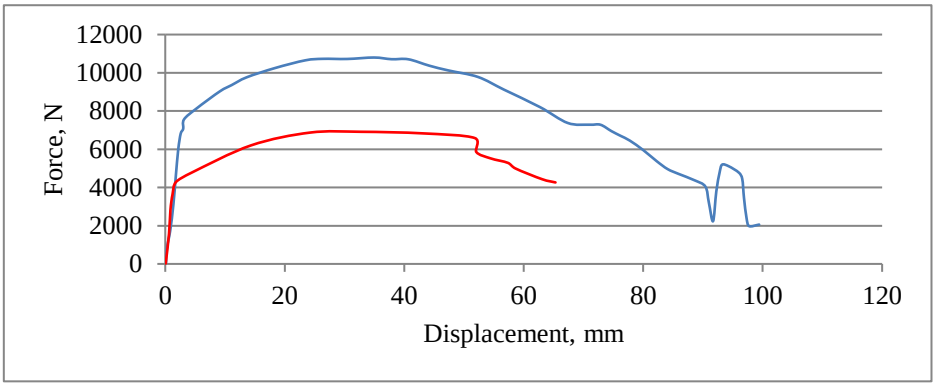

Fig. 12. Comparison of diagrams welded specimen and rolled.

The results of the bending test are shown in figure 4. The changes at the end of the welding specimen diagram were due to the specimen's movement on the lower jaw of the machine at the end of the bending load. No trace of cracking and discontinuity was observed in the specimens after the test. Based on the relations (12) to (17), for analytical calculations, the applied stress is first calculated to calculate the moment of inertia of the surfaces, and then the bending stress is obtained. (Dimensions in mm). The results of the static bending test are shown in figure 13 according to pressure strength and ultimate yield. Figure 13 shows specimen dimensions for calculating the center of the surface and bending stress. Figure 14 shows the final image of the specimen under bending, and the hardness of the specimen tested is calculated in Rockwell.

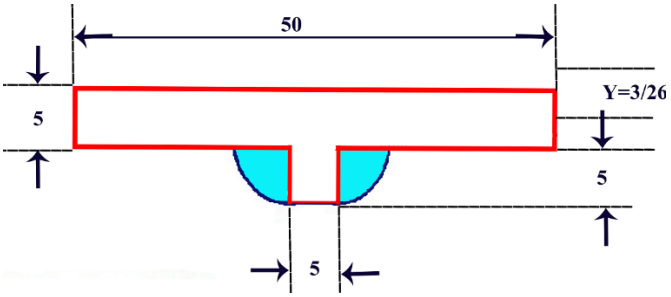

Fig. 13. Specimen dimensions for calculating the center of the surface and bending stress.

Fig. 14. The final image of the welded specimen under bending.

$$\bar{Y} = \frac{1}{A}\sum \bar{y}_i . A_i = \frac{1}{250+25+25}(250\times 2/5 + 25\times 7/5 + 25\times 6/66) = 3/263 \text{mm} \quad (12)$$

$$I_{X'} = \sum(\bar{I} + Ad^2) = 520/83 + 145/88 + 500/71 + 313/05 = 1480/47 \text{mm}^4 \quad (13)$$

$$\sigma = \frac{MC}{I} = \frac{7500\times 250\times 3/263}{4\times 1480/47} = 1033/13 \text{ MPa} \quad (14)$$

$$\sigma = \frac{MC}{I} = \frac{10916/18\times 250\times 3/263}{4\times 1480/47} = 1503/72 \text{ MPa} \quad (15)$$

$$\sigma = \frac{MC}{I} = \frac{4556\times 250\times 3/263}{4\times 1480/47} = 627/59 \text{ MPa} \quad (16)$$

$$\sigma = \frac{MC}{I} = \frac{7181/34 \times 250 \times 3/263}{4 \times 1480/47} = 989/24\ \text{MPa} \qquad 17$$

The average hardness of the base metal of the welded specimen 73.25B and the hardness of the rolled specimen 80.83B have been calculated. The results of the hardness test are given in figure 15. The above data are calculated statistically based on the relations (1), (2), (3), and (4), the results of which are presented in figure 16. Figure 17 shows hardness test results (BRH).

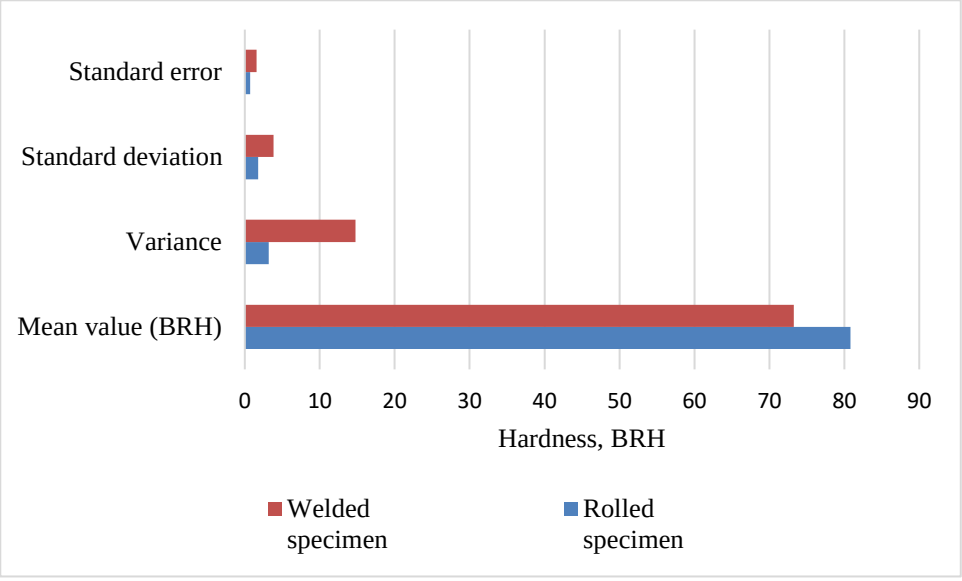

Fig. 15. Statistical analysis of hardness results.

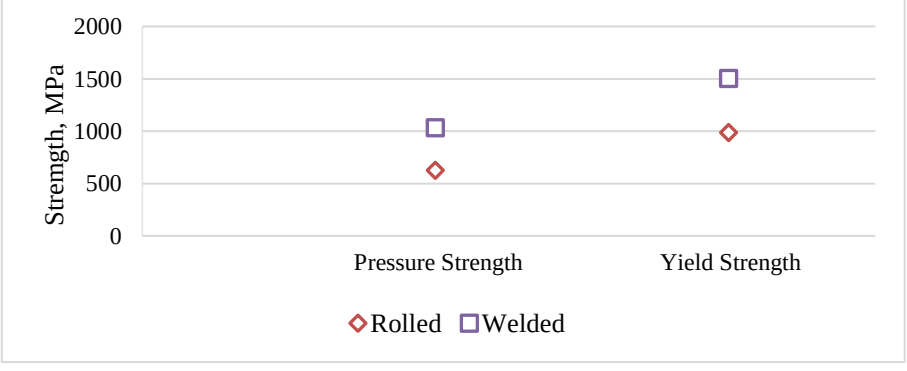

Fig. 16. The results of the static bending test

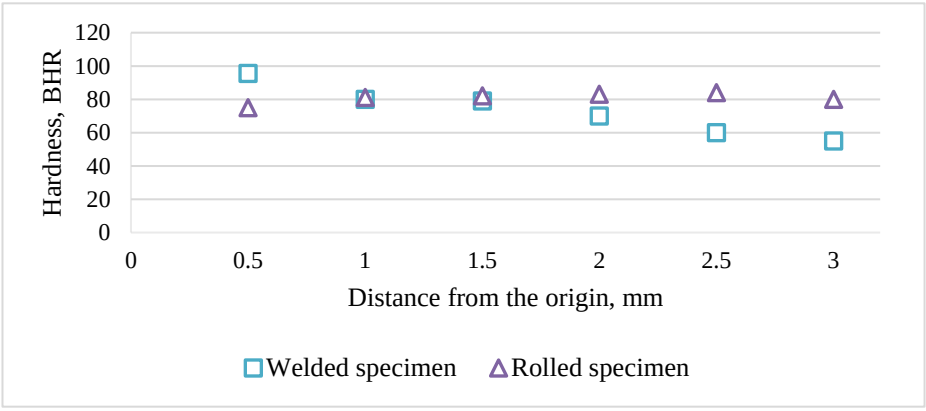

Fig. 17. Hardness test results (BRH).

The values obtained from the mean hardness of the specimens, it is determined that the hardness of the rolled specimen is higher than the welded specimen, and the reason may be due to the low amount of carbon in the weld metal composition. The hardness profile diagrams in Figure 18 are due to the welding operation and the formation of a heat-affected area on a specimen. According to the heat applied in the welding process, the base metal undergoes heat treatment and its microstructure changes. The base metal grains become smaller, and as a result, their hardness increases. The lower the weld root to the weld surface, the lower the metal's hardness, but in the rolled specimens is the opposite. Due to the amount of variance and standard deviation that the scattering of hard results is lower than the mean value, the rolled specimen is less than the welded specimen. Performing rolling operations on T-Bar profile profiles by smoothing the grains helps to improve mechanical properties such as hardness. Therefore, the reduction in the scattering of hardening results in these points can be due to the uniformity of the grains.

Figure 18 shows a welded specimen that has failed after 313214 cycles. While the rolled specimen continued for up to 2 million cycles under fatigue load and no failure was obtained in the rolled specimen. The loading conditions were based on Table 2 the choice of fatigue loading value for each specimen was based on 90% of the yield stress value of the specimens. The welded specimen in cycle 3×105 fails with these stress levels, while the rolled specimen enters the unlimited life range. The reasons for the failure of the specimen in the metallurgical and fracture tests have been discussed below.

Fig. 18. Welded specimen after failure.

Using relations (3) to (10), the stress levels used in the bending test are shown in Table 3 based on the highest and lowest load values. The following fatigue variables are calculated.

Table 2. Min and max stress levels in the fatigue test.

	Min stress level (MPa)	Max stress Level (MPa)	Min loading Level (N)	Max Loading Level (N)	Loading Type
Welded specimen	110.20	964.26	800	7000	Sine
Rolled specimen	110.20	551.01	800	4000	Sine

$$\Delta\sigma = \sigma_{max} - \sigma_{min} = -964/26 - (-110/20) = -854/06 \text{ MPa} \quad (18)$$

$$\Delta\sigma = \sigma_{max} - \sigma_{min} = -551/01 - (-110/20) = -440/81 \text{MPa} \quad (19)$$

$$\sigma_a = \frac{\sigma_{max} - \sigma_{min}}{2} = \frac{-964/26 - (-110/20)}{2} = -427/03 \text{MPa} \quad (20)$$

The values obtained from the fatigue variables of the welded and rolled specimens are shown in Figure 19.

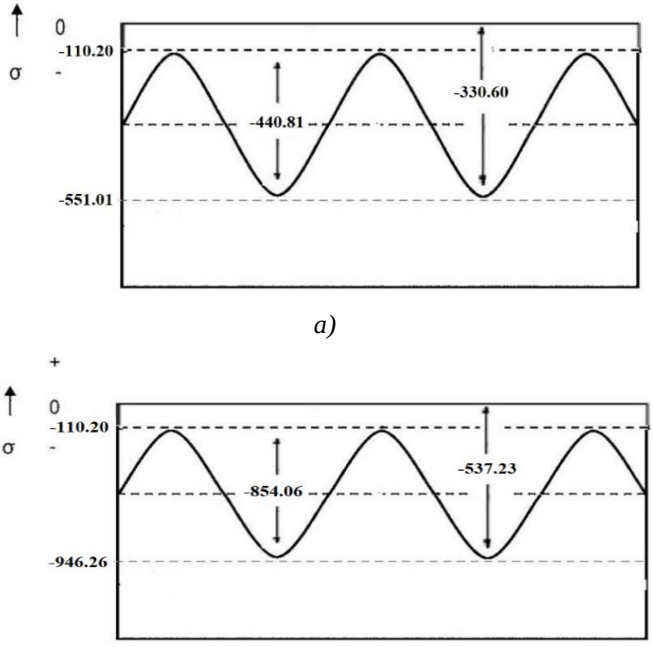

a)

b)

Fig. 19. a) Diagram of fatigue variables in the Rolled specimen, b) and in the Welded specimen.

$$\sigma_a = \frac{\sigma_{max} - \sigma_{min}}{2} = \frac{\text{-}551/01 - (\text{-}110/20)}{2} = \text{-}220/40\text{MPa} \quad (21)$$

$$\sigma_m = \frac{\sigma_{max} + \sigma_{min}}{2} = \frac{\text{-}964/26 + (\text{-}110/20)}{2} = \text{-}537/23\text{MPa} \quad (22)$$

$$\sigma_m = \frac{\sigma_{max} + \sigma_{min}}{2} = \frac{\text{-}551/01 + (\text{-}110/20)}{2} = \text{-}330/60\text{MPa} \quad (23)$$

$$R = \frac{\sigma_{min}}{\sigma_{max}} = \frac{110/20}{964/26} = 0/114 \quad (24)$$

$$R = \frac{\sigma_{min}}{\sigma_{max}} = \frac{110/20}{551/01} = 0/199 \quad (25)$$

$$A = \frac{\sigma_a}{\sigma_m} = \frac{427/03}{537/23} = 0/79 \quad (26)$$

$$A = \frac{\sigma_a}{\sigma_m} = \frac{220/40}{330/60} = 0/66 \quad (27)$$

$$\Delta\sigma = \sigma_{max} - \sigma_{min} \quad (28)$$

$$\sigma_a = \frac{\sigma_{max} - \sigma_{min}}{2} \quad (29)$$

$$\sigma_m = \frac{\sigma_{max} + \sigma_{min}}{2} \quad (30)$$

$$R = \frac{\sigma_{min}}{\sigma_{max}} \quad (31)$$

$$A = \frac{\sigma_a}{\sigma_m} \quad (32)$$

Scanning Electron Microscope (SEM) images of the fracture surface are shown in Figure 20. After cross-cutting, the sanding is determined a little farther from the site of failure of the stress concentration centers in the welded area. Figure 21 shows stereo-microscope images of the fracture surface and the stress concentration points in the welded area. Slightly farther from the refractive surface, for further investigation after imaging by optical microscopy, images were obtained that were characterized by different large-scale cracks at the end of the vertical sheet and no weld. Figure 22 shows Optical microscopy images of crack propagation on the fracture surfaces. To further investigate the fracture local, images were taken using an electron microscope. To determine the structure of the base metal and the fracture structure and determine the size of the ferrite grain, SEM images of the welded fracture specimen that has been tested for fatigue are shown in Figure 22. The size of the ferrite grain determined from the metal structure is ASTM E 112, equal is 10 [27]. Due to the non-welding area at the end of the vertical sheet, the welding parameters of the sheets with the T-Bar profile joint are investigated in this section. Figure 23 shows the welding parameters according to standard 131540B

[27]. The values obtained from these parameters for the sheet with a thickness of 5 mm are shown in Table 3 according to the measured values, the welding parameters are in terms of penetration depth according to the standard. Still, the non-weld ability is seen as a hole at the two ends of the vertical plate connected to the following plate, which can be the starting point of failure. Depending on the type of loading, the edges of the top sheet of chamfer appropriate should be created using the full weld design, and the distance between the root of the sheet should be such that the weld penetration is complete and strong. Connecting the vertical plate to the bottom plate can act as a weak point in vibrational cycles. At both ends of the vertical sheet, the focus of tension is created, causing cracks and eventually failure of the workpiece. According to the results of fatigue and bending tests, it can be considered that in cases where a T-Bar profile joint is required for the structure, if the structure is under load loading with less load, the use of T-Bar profiling profiles is more durable than welded T-Bar profile joints. Also, suppose the joint of the welded T-Bar profile is used for the structure while considering the number of cycles and the amount of loading. In that case, the appropriate arch should be used to fill the joint of the roots of the sheets and eliminate the stress concentration points.

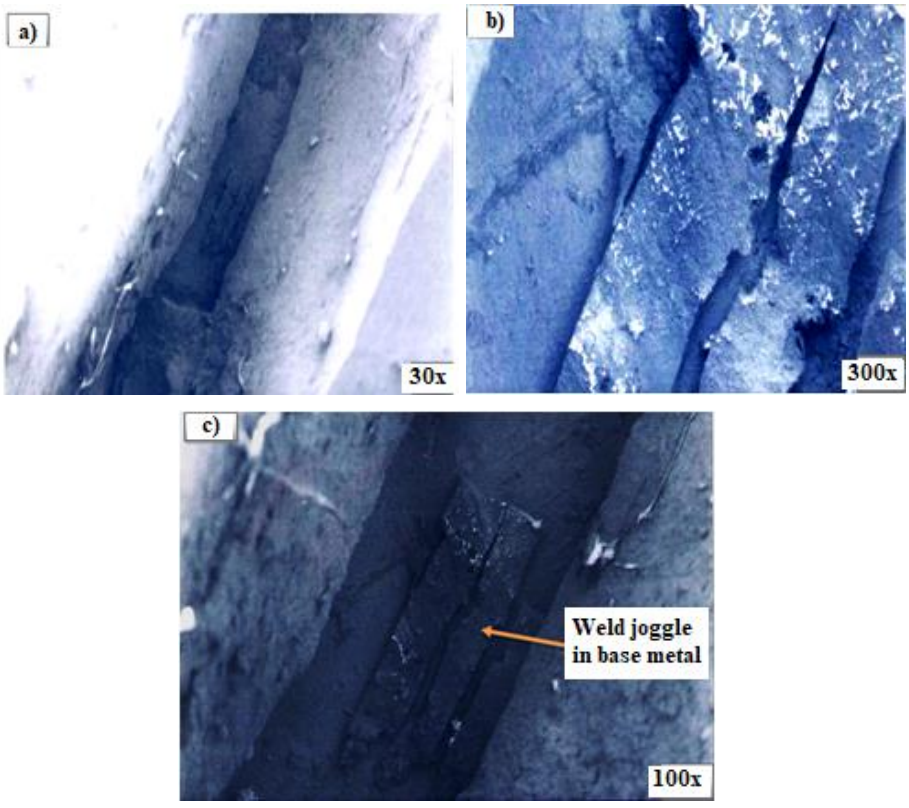

Fig. 20. Scanning Electron Microscope (SEM) images of the fracture surface.

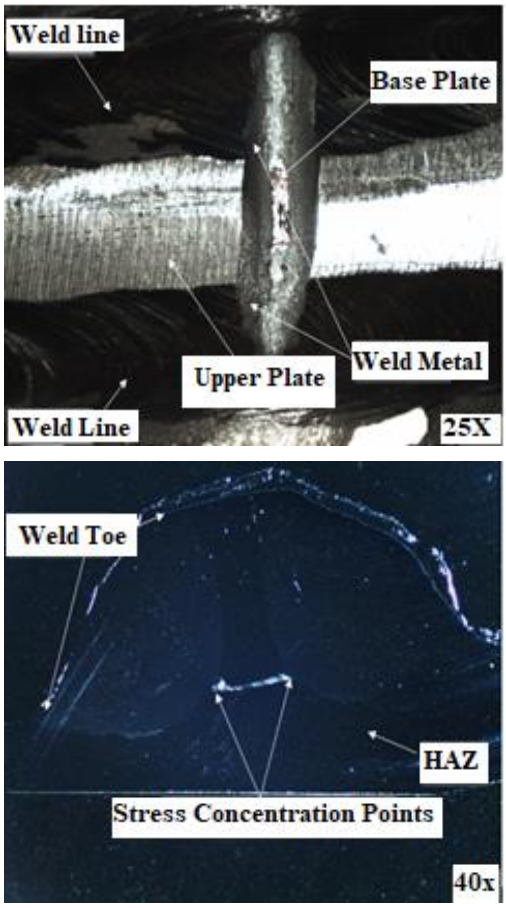

Fig. 21. Stereo-microscope images of the fracture surface.

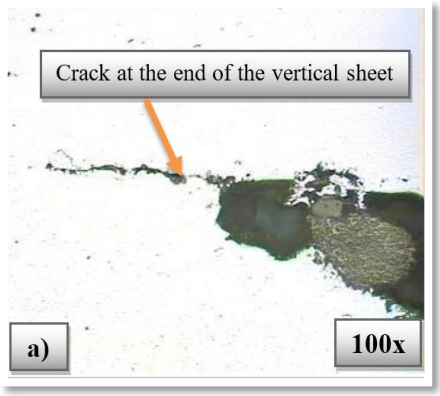
Crack at the end of the vertical sheet
a)
100x

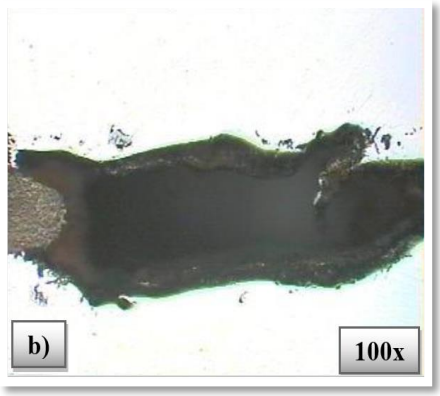
b)
100x

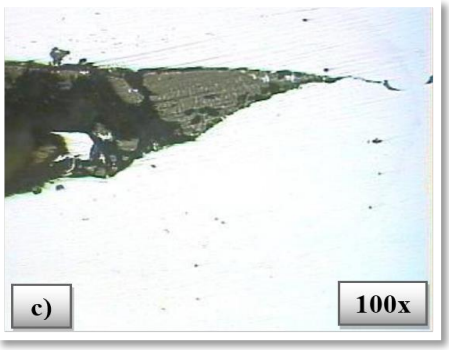
c)
100x

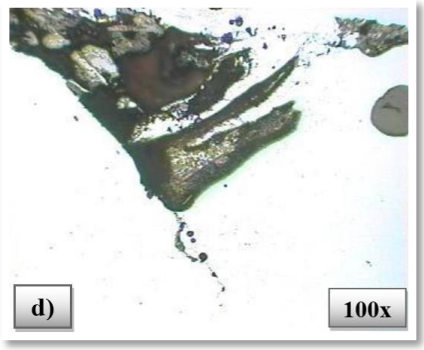
d)
100x

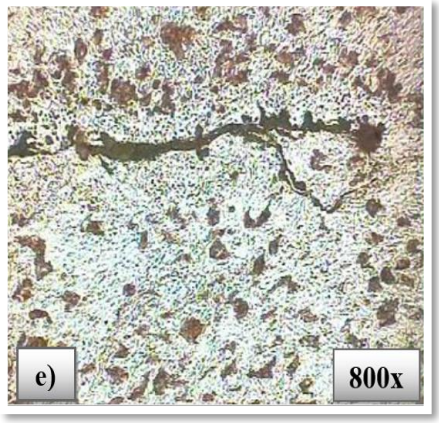
e)
800x

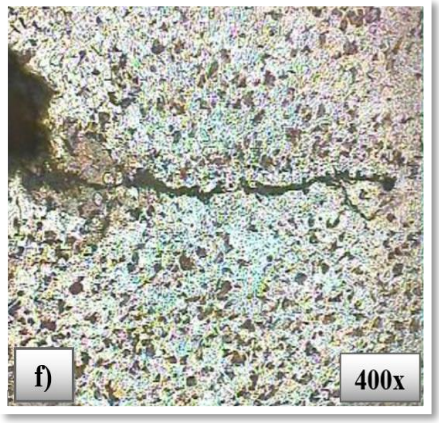
f)
400x

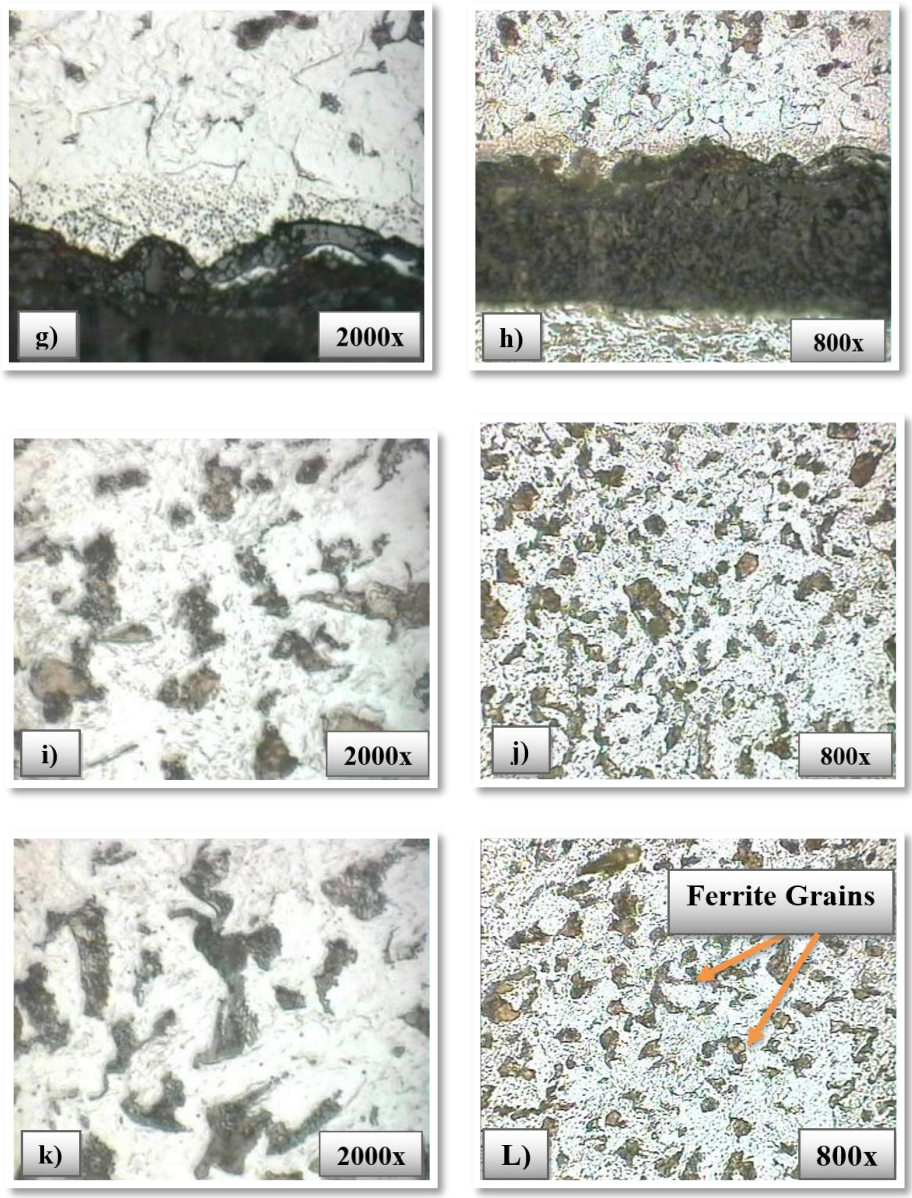

Fig. 22. Optical microscopy images of crack propagation on the fracture surfaces.

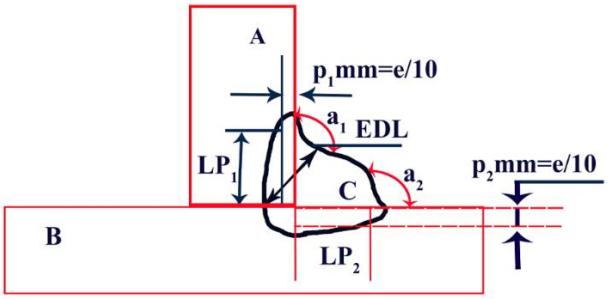

Fig. 23. Welding parameters.

Table 3. Values of welding parameters for the specimen.

	EDL (mm)	LP2 (mm)	LP1 (mm)
Right side welding	7.5	6.5	7
Left side welding	7.7	7.5	7.4
Allowable range	> = 5	> = 5	> = 5

Conclusion

In this study, the effect of applied stress on the properties of High Cycle Fatigue was investigated in welded specimens with T-Bar profiled joint design and rolled T-Bar profiled steel profile specimen, and the following results were obtained:

1) Despite the standard welding parameters, non-welding at both ends of the vertical plate connected to the bottom plate can be the starting point for failure.
2) Connecting the vertical plate to the bottom plate can act as a weak point in vibrational cycles, and at both ends of the vertical sheet, the focus of tension is created, causing cracks and eventually failure of the part.
3) Due to stress concentration at the end of the joint between the two sheets and the creation of cracks, this joint design cannot tolerate vibrational cycles.
4) In the case of using a full penetration welding joint design, depending on the type of loading, the edges of the upper sheet of the appropriate patch should be created, and the distance between the root of the sheet should be sufficient to create a complete and strong weld penetration.
5) Welded specimens have a higher bending strength than T-Bar profiled specimens.
6) Welded specimens have a lower hardness than thermal profile specimens due to their thermal and welding processes and low carbon content.
7) If you have used a welded joint for the structure, you must use the appropriate arc to fill in the joint of the root of the sheets and eliminate the stress concentration points, taking into account the number of cycles and the amount of loading.

8) With the fillet weld joints, it is necessary to under loading of the high cycle with a lower load. The use of T-Bar profiles is more durable than of T-Bar welded joints.

Acknowledgment

The fatigue test was performed in the vibration and fatigue laboratory of the testing and research company of automobile parts and assemblies (Itrak).

Appendix

Latin signs

Equivalent carbon	CE
Chemical Components	P_{cm}
Number of cycles in loading	N
The tension level in loading	S
Tension ratio	R
Intermittent stress ratio	A
Length of cracks	da
Average value	$\bar{x}$
Variance	S^2
Standard deviation	S
Medium standard error	$S_{\bar{x}}$

Greece signs

Average stress	σ_m
The range of stress	$\Delta\sigma$
Maximum stress	$\sigma_{\max}$
Minimal stress	$\sigma_{\min}$
Load strain	ε
The intensity of the tension	ΔK

References

[1] H. Zenner, K. Hinkelmann: Steel Construction, 12 (2019) 156-162.
[2] K. Jud, H. Kausch, J. Williams: Journal of Materials Science ,16 (1981) 204-210.
[3] M. Torkamany, S. Tahamtan, J. Sabbaghzadeh: Materials & Design, 31 (2010) 458-465.
[4] K. Hong, C. Yung: Journal of Materials Processing, 245 (2017) 46-69.
[5] D. Yaschenko, A. Dmitry, S. Chinakhov: Advanced Materials Research, 1040 (2014) 837-844.
[6] R. Hertzberg, H. Saunders: Construction Materials (1985) 309-311.
[7] Y. Huang, W. Yaobin, W. Long: The International Journal of Advanced Technology, 87 (2016) 1115-1123.
[8] B. Wilczynski, Z. Mroz: Computers & structures, 85 (2007) 1382-1398.

[9] W. Becker, J. Roch, S. Shipley, R. Lampman, R. Bonnie: ASM handbook, 11: 1072. ISBN: 0-87170-704-7, (2002).
[10] L. Chen, A. Cernicchi, M. Gilchrist, F. Cardiff: Materials & Design, 162 (2019) 106-118.
[11] J. Dearden: Institute of Welding Transactions, 3 (1940) 203.
[12] G. Sih, N. Ryan, R. Jones: International Conference on Fracture Mechanics Technology Applied to Material Evaluation and Structure Design, (2012), 10–13.
[13] Lenard, John G. Primer on flat rolling. Newnes, ISBN: 9780080994123, (2013).
[14] American Welding Society. Structural Welding Committee, American National Standards Institute, and Welding Society. Technical Activity Committee. Structural Welding Code--steel. American Welding Society, 1994.
[15] X. Zhi-Gang, K. Yamada: International Journal of Fatigue, 26 (2004), 1277-1293.
[16] R. Guchinsky, V. Sergei: Magazine of Civil Engineering, 4 (2011) 5-9.
[17] B. Biehn, K. Yamada, T. Ishikawa: International Journal of Steel Structures 8, (2008) 163-169.
[18] E. Ahmet, F. Sonmez: Finite Elements in Analysis and Design, 47 (2011) 413-423.
[19] P. Haslberger, S. Holly, W. Ernst, R. Schnitzer: Journal of materials science 53 (2018) 6968-6979.
[20] L. Huang, H. Xueming, W. Dongsheng, L. Fang: Journal of Materials Processing Technology, 252 (2018) 421-431.
[21] P. Chandan, M. Mahapatra, P. Kumar, N. Saini: Materials Science and Engineering A, 712 (2018) 720-737.
[22] G. Alessio, P. Matteis, F. D'Aiuto: Metals, 9 (2019) 315.
[23] R. Stephens, A. Fatemi, H. Fuchs: John Wiley & Sons. ISBN: 978-0-471-51059-8, (2000).
[24] AM. Petrudi, M. Rahmani: Revue des Composites et des Matériaux Avancés-Journal of Composite and Advanced Materials, 30 (2020) 61-68.
[25] M. Wojciech, R. Branco, J. Trembacz, J. D. Costa, J. Ferreira, C. Capela: Engineering Failure Analysis, 118 (2020) 104-784.
[26] M. Wojciech, R. Owsiński, J. Trembacz, R. Branco: Mechanics of Materials, 147 (2020) 103-410.
[27] ASTM, C: American Society for Testing Materials, (1958).
[28] A. Ahmet, A. Şik: Mechanical Fatigue of Metals, 7 (2019) 343-349.
[29] Maine Welding Company, Welding Positions, https://mewelding.com/welding-positions, Accessed April 2021.